Applications of the atomic force microscopy to nuclear track methodology

C. Vázquez-López and R. Fragoso
Departamento de Física. Centro de Investigación y de Estudios Avanzados.
Apartado Postal 14-740, 07000, México, D.F.
cvlopez@fis.cinvestav.mx

J.I. Golzarri and G. Espinosa
Instituto de Física, Universidad Nacional Autónoma de México.
Apartado postal 20-364, 01000 México, D.F.
espinosa@fisica.unam.mx

Recibido el 2 de marzo de 2006; aceptado el 18 de agosto de 2006

The fundamental instrumentation scheme of atomic force microscopy is reviewed, with the purpose of understanding the great value of this technology in studying nuclear tracks in solids. Different morphologies are revealed in the samples, in which detailed metrological features are very important in the characterization and study of nuclear tracks. Among them, conical pits on etched CR-39 exposed to alpha particles, and hillocks and/or craters on some minerals exposed to ^{252}Cf fission fragments. Some examples of artifacts in the convolution of sample topography and probe geometry are also mentioned.

Keywords: Atomic force microscopy; nuclear track detectors; plastic detectors.

Se revisa el esquema fundamental de la instrumentación de la microscopía de fuerza atómica, con el propósito de entender el gran valor de esta tecnología en el estudio de las trazas nucleares en sólidos. Diferentes morfologías aparecen en las muestras, en las que se determinan detalles metrológicos muy importantes en la caracterización y estudio de las trazas. Entre ellas están los orificios cónicos en CR-39 revelados químicamente después de la exposición a partículas alfa, y las montañas y/o cráteres sobre algunos minerales expuestos a fragmentos de fisión del ^{252}Cf. Algunos ejemplos de artefactos que aparecen en la convolución de la topografía de las muestras con la geometría de las puntas de prueba son también mencionados.

Descriptores: Microscopio de fuerza atómica; metodología de trazas nucleares; detectores plásticos.

PACS: 07.79.Lh, 07.57.Kp, 29.40. –n, 85.25.Pb

1. Introduction

The atomic force microscope (AFM), invented 20 years ago by Binnig et al. [1], is a metrologic instrument belonging to the family of scanning probe microscopes, which has more than twenty members these days. In this work, the fundamental instrumentation scheme of AFM is reviewed, with the purpose of understanding the great value of this technology in studying nuclear tracks in solids.

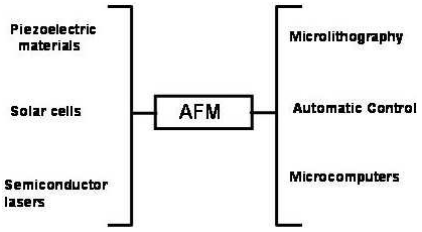

FIGURE 1. Technologies that gave rise to SPM instrumentation.

2. AFM basics

A diagram of the technological achievements that gave rise to the scanning probe microscopes is presented in Fig. 1. The heart of this instrumentation is the piezoelectric scanner positioner, which permits the x-y scanning process and the controlled interaction between the surface sample and the probe. In Fig. 2, a scheme of a typical design of a piezoelectric actuator is shown. It consists in a cylindrical shell with 4 lateral electrodes labeled X, -X, Y, and –Y, and a ground electrode deposited on the inner cylindrical surface. When the four lateral electrodes are connected to the same bias, the cylinder extends. On the opposite polarity, it retracts. This is the z-axis movement which is a control system response. The x-y movements corresponding to the scanning process are obtained by applying programmed biases to the lateral electrodes.

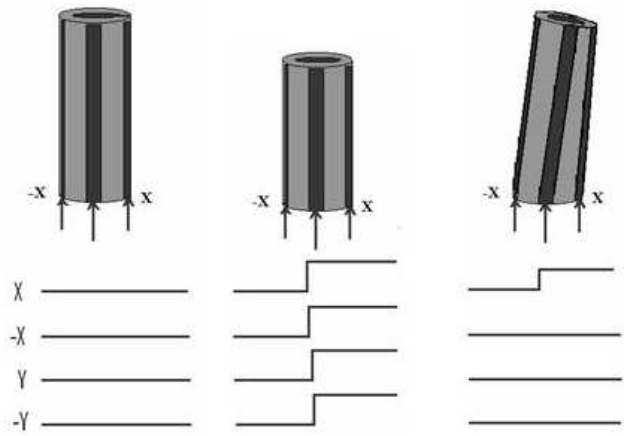

FIGURE 2. A typical design of the piezoelectric actuator, on which the sample is placed.

The system uses three DACs for the control of scanning, scaling, and z-offset of each scan axis (x,y,z). The movement in Fig. 2 has been exaggerated, for clarity.

In order to review the way in which an AFM works, let us make a didactical toy using the technologies mentioned before. In Fig. 3, the diagram of an optical sensor with a piezoelectric transducer is shown. The optical sensor consists in a double-sector photodetector whose outputs are applied to a differential operational amplifier (op-amp). The output of this op-amp is buffered to bias the z-movement of a cylindrical piezoelectric actuator. When a laser beam incides on the central region of the composed photodetector, there is no voltage at the op-amp output. However, small shifts of the beam are transduced in extensions or retractions of the piezoelectric actuator, in response to the applied electric potential, since the op-amp output is proportional to the difference in light intensity on the photodetector sectors. This basic optical position sensor is used in the diagram shown in Fig. 4.

The sample surface sensor, typically a triangular shaped cantilever with a probe tip in contact with the sample, reflects the laser beam towards the optical position sensor. The size of the cantilever is 0.3 mm long. The tip normally is conical, with a radius of curvature of 10 nm. In Fig. 5, a SEM image of a tip probe of the Ultralever type (from Digital Instruments) is shown.

The basic schematics of the AFM system shown in Fig. 4, has a feedback controller with an established gain in order to prevent chaotic oscillations. The probe signal VA – VB is compared (subtracted) with a set point corresponding to the contact force (of the order of nanonewtons). This difference is called error signal, and is added to the feedback controller, where it is amplified according to the gain chosen by the operator. Then, the output is used to bias the z-axis movement of the piezoelectric actuator to compensate the surface feature of the sample at that point. The same voltage applied to the z-component of the actuator is used to generate the corresponding height of the image pixel on the screen. Previously, the system is programmed by the operator with the following parameters: a) size of the scanning surface, b) contact force (set point), c) number of pixels (256×256 or 512× 512), d) piezoscanner calibration, e) scanning frequency, f) feedback gain, g) image slope compensation. It is remarkable the servomechanism feature of the system, that almost simultaneously scans the surface and compensates the z component to follow the sample topography [2].

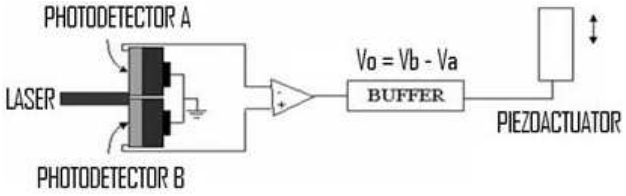

FIGURE 3. The basic response mechanism of an AFM.

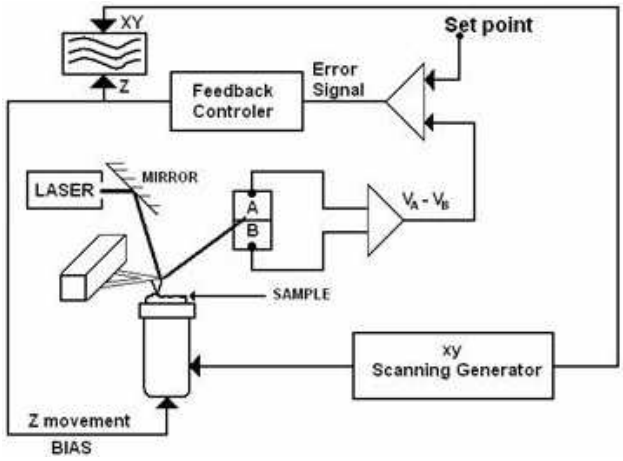

FIGURE 4. AFM system basic schematics.

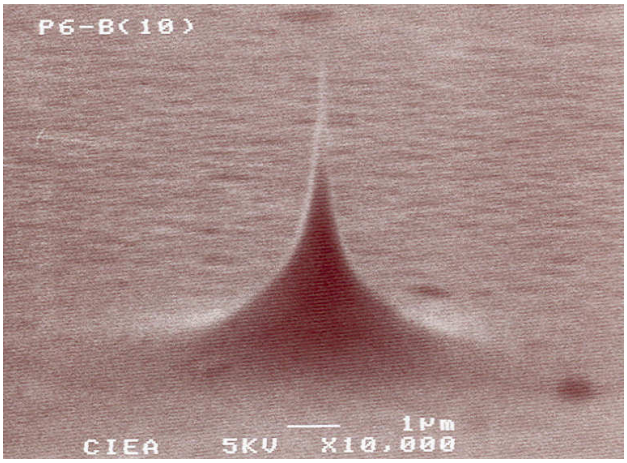

FIGURE 5. The tip probe, of the ultralever type.

The difference in track diameters can be observed directly from the images, and the depth can be measured using the height profile.

3. Examples of the use of AFM in the nuclear track methodology.

3.1. Conical pits on CR-39

Fig. 6 shows two AFM images of nuclear tracks induced by alpha particles of 5.15 MeV from a ^{239}Pu source incident on CR-39 Lantrack®polycarbonate, etched during 30 minutes (Fig. 6a) and 1 hour (Fig. 6b), in 6.25 M KOH, at 60°C [3, 4].

3.2. Craters and ejected material produced by nuclear fission fragments

Three target materials were investigated: a natural diamond of about 1 mm, a natural quartz crystal, and a commercial silica optical fiber (Nokia fiber). The radiation source was ^{252}Cf with an activity of 98 fission fragments (ff) per min/cm^2. Irradiations were made in air and collimated approximately normal to the target surface.

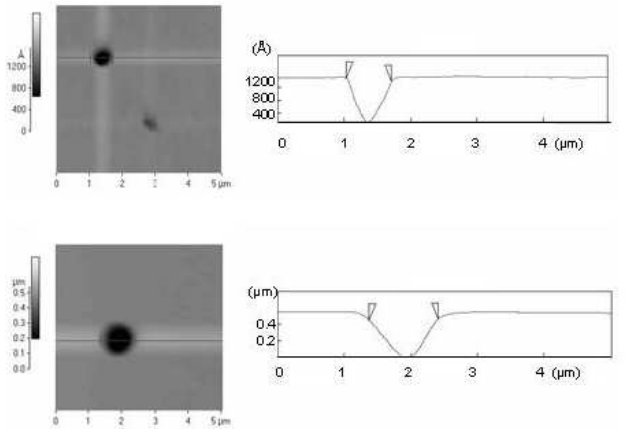

FIGURE 6. AFM images of alpha nuclear tracks on CR-39, etched during 30 minutes and 1 hour. A topographic profile along the indicated line is also shown for each image.

The calculated rate of surface impacts was 1 ff per week per area of 10,000 microns^2. Irradiations were made for up to 20 days and produced about 5 impacts per zone observed in the AFM.

AFM micrographs of diamond surface, before and after irradiation, are shown in Fig. 7a, and 7b; three impact craters are shown in 7b. We can recognize two parallel rows of hillocks, the more distinct row being the one closest to the line of impact craters. The scale shows that the irregularly shaped craters have dimensions of up to a few microns, while the hillocks appear to be a few tenths of microns in size, up to a maximum of 0.5 microns. Craters of a similar nature have been observed by AFM in other organic crystals such as benzoyl glycene [5].

Views of unirradiated and irradiated quartz are shown in Fig. 8a and 8b, respectively. Impacts result in a well-developed array of rounded hillocks, in the size range 0.05 to 0.2 microns, and in a distinct x-y array (Fig. 8b). There is little evidence of any impact cratering, in contrast to the situation with diamond. The unirradiated quartz surface (Fig. 8a) shows a smooth topology with features on the order of 10 Å.

Fig. 9 has the analogous AFM micrographs of amorphous silica fiber. The original fiber surface (Fig. 9a) is smooth and on the order of over 15 Å. After irradiation with ff's, a random pattern of hillocks is clearly seen (Fig. 9b), with heights of up to 0.07 microns.

4. Limitations. Image artifacts

There are four primary sources of artifacts in images measured with atomic force microscopes. They are: probes, scanners, image processing, and vibrations.

The probe artifacts are the most common problem in nuclear track methodology. These artifacts are produced by two geometrical features of the probe: the length of the probe and the shape and dimensions of the tip.

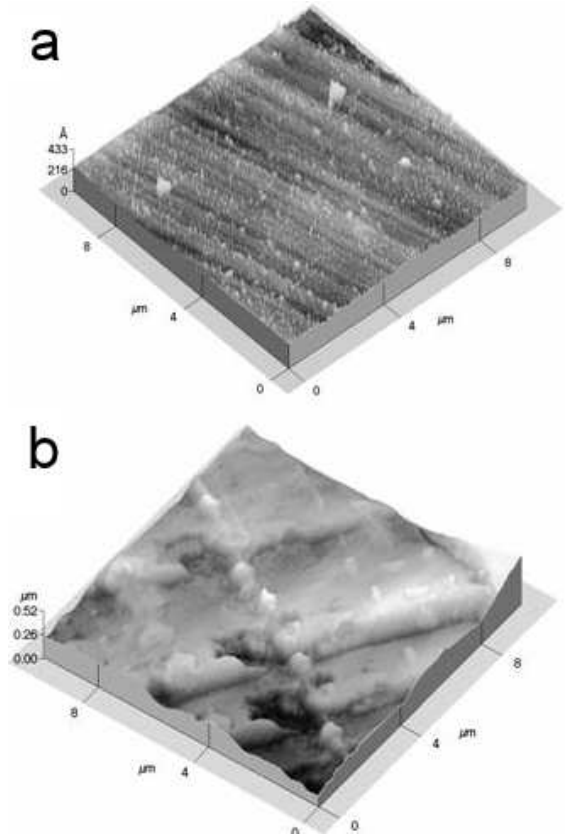

FIGURE 7. Diamond surface images a) unirradiated, and b) irradiated.

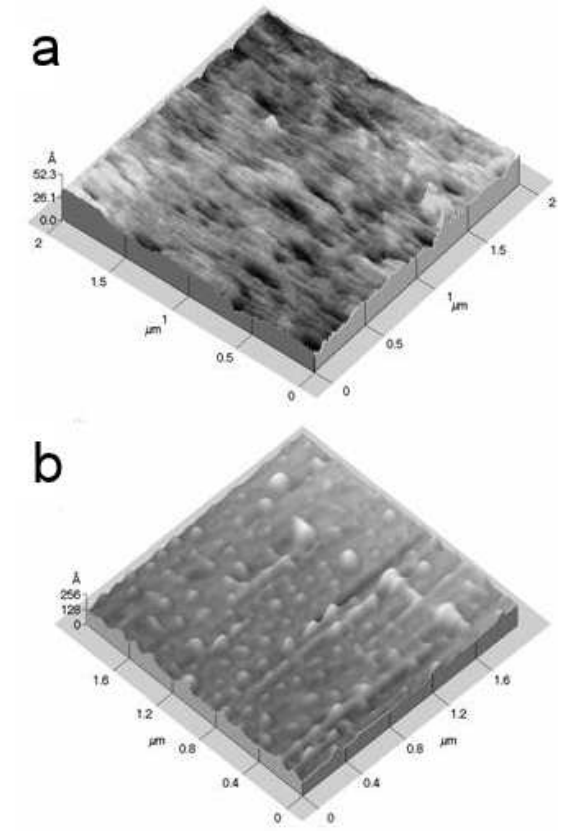

FIGURE 8. Quartz surface: a) unirradiated, and b) irradiated.

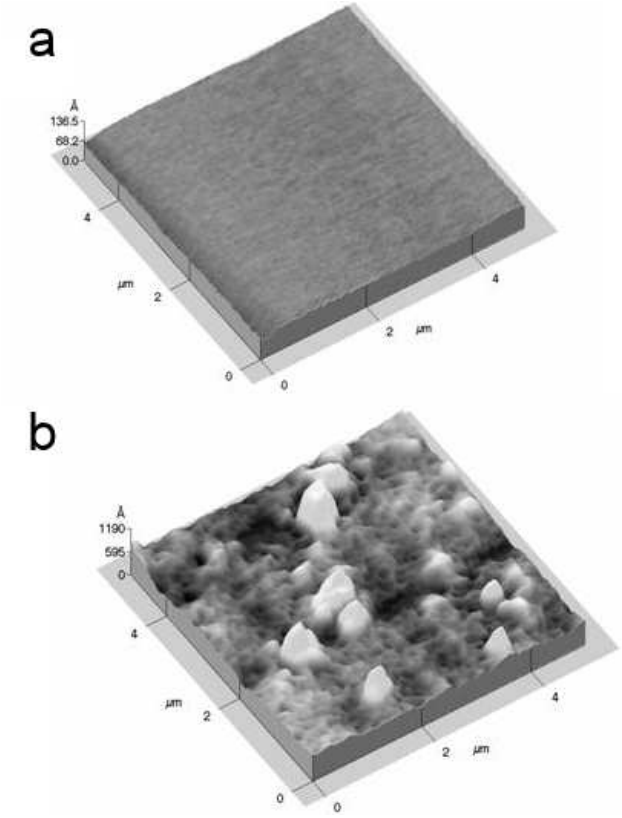

FIGURE 9. Optical fiber surface: a) unirradiated, and b) irradiated.

When the length of the probe is too short, for example in pyramidal tips called microlevers, the artifact shown in Fig. 10 appears. Truncated cones are obtained in CR-39. The reason for this artifact is that in this case, a probe tip 2 microns in height was used. It is clear that these kinds of tips are not reliable for scanning tracks with etching times longer than 3 hours, since the cantilever impedes the continuous contact of the probe tip with the sample in the scanning process.

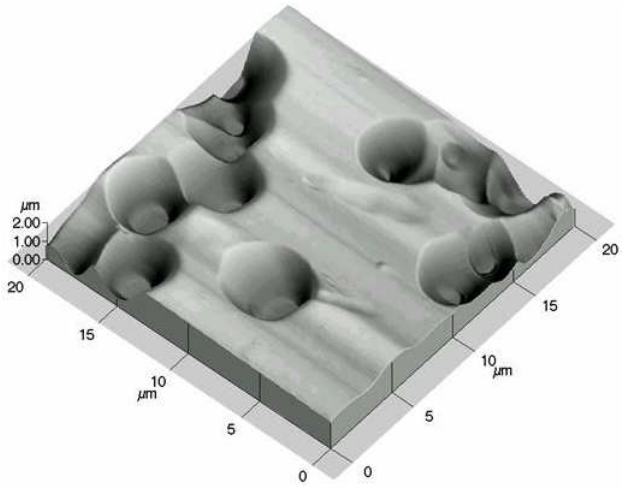

FIGURE 10. AFM of some alpha tracks on CR-39, etched during 4 hours. The truncated cones are probe artifacts.

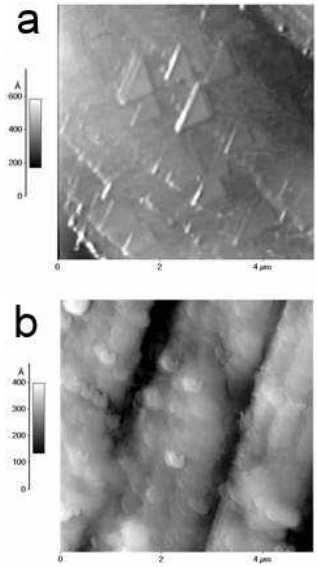

FIGURE 11. AFM images of aquamarine mineral irradiated with ^{252}Cf fission fragments. Fig. 11a was taken with a truncated pyramidal tip. Fig. 11b corresponds to the same sample taken with an ultralever probe.

The shape of the tip is also crucial. Fig. 11 shows the effect of using a truncated pyramidal tip for samples with ejected material due to fission fragments. Artifacts appear as triangular features, revealing the shape of the probe tip. In this case, the tip is acting as the sample, and the hillocks as the tip.

5. Conclusions

An easy explanation of the AFM basic operation has been reviewed. This instrumentation is very reliable for studying nuclear tracks on solids. For CR-39 exposed to alphas, a minimum etching time is necessary. For diamond and quartz exposed to ^{252}Cf fission fragment particles, craters were observed, in the case of diamond, and ejected material for both, deposited on ordered sites. For amorphous silica, the ejected material was deposited randomly. The materials reported show different behavior upon exposure to ionizing radiation. For CR-39, the precise description of the nuclear alpha latent track is an open question still. For the materials exposed to fission fragments, the sputtering process must be carefully studied, since irradiations in air may have allowed the cratering in carbon to be oxydatively enhanced.

In AFM instrumentation, it is very important to be aware of the possible image artifacts that might show up due to the shape and relative dimensions of the AFM probe tip. For nuclear track methodology, it is necessary to use probe tips of high aspect ratio.

Acknowledgements

The authors thank the technical assistance of Blanca Zendejas and Ana Bertha Soto.

1. G. Binig, C.F. Quate, and C. Gerber, *Phys. Rev. Lett*. **56 (**1986) 930
2. Digital Instruments Tutorial.
3. G. Espinosa, I. Jacobson, J.I. Golzarri, C. Vazquez, R. Fragoso, and E. Santos, *Radiation Protection Dosimetry*, **101** (2002) 89.
4. C. Vázquez-López, R. Fragoso, J.I. Golzarri, F. Castillo-Mejía, M. Fujii, and G. Espinosa, *Radiation Measurements*, **34** (2001) 189.
5. H.S. Nagaraje, F. Ohnesorge, D.K. Avasthi, , R. Neuman, P. Mohan-Rao, *Appl Phys. A*, **71** (2000) 337.